Ultrathin Gold Nanowires: Soft-Templating versus Liquid Phase Synthesis, a Quantitative Study

Anais Loubat, Lise-Marie Lacroix, Antoine Robert, Marianne Imperor-Clerc, Romuald Poteau, Laurent Maron, Raul Arenal, Brigitte Pansu, G. Viau

Ultrathin Au Nanowires: Soft-Templating vs Liquid Phase Synthesis, a Quantitative Study.

Journal:	*The Journal of Physical Chemistry*
Manuscript ID:	jp-2015-00242n.R1
Manuscript Type:	Article
Date Submitted by the Author:	n/a
Complete List of Authors:	Loubat, Anaïs; Laboratoire National des Champs Magnétiques Intenses, CNRS-INSA-UJF-UPS, UPR3228; Université de Toulouse, INSA, UPS, LPCNO Lacroix, Lise-Marie; Université de Toulouse, INSA, UPS, LPCNO; Transpyrenean Advanced Laboratory for Electron Microscopy (TALEM), INSA - INA, CNRS - Universidad de Zaragoza, Robert, Antoine; Université de Toulouse, INSA, UPS, LPCNO Impéror-Clerc, Marianne; Université Paris Sud, Poteau, Romuald; INSA Toulouse, LPCNO; LPCNO-IRSAMC, Maron, Laurent; INSA, Université Paul Sabatier, Laboratoire de Physique et Chimie des Nanoobjets Arenal, Raul; Universidad de Zaragoza, Instituto de Nanociencia de Aragon; Fundacion ARAID, ; Transpyrenean Advanced Laboratory for Electron Microscopy (TALEM), INSA - INA, CNRS - Universidad de Zaragoza, Pansu, Brigitte; Universite PARIS SUD, Laboratoire de Physique des Solides Viau, Guillaume; INSA Toulouse, LPCNO; Transpyrenean Advanced Laboratory for Electron Microscopy (TALEM), INSA - INA, CNRS - Universidad de Zaragoza,

Ultrathin Au Nanowires: Soft-Templating vs Liquid Phase Synthesis, a quantitative study.

Anaïs Loubat,[a,b] Lise-Marie Lacroix,[a,c] Antoine Robert,[a] Marianne Impéror-Clerc,[d] Romuald Poteau,[a] Laurent Maron,[a] Raul Arenal,[c,e,f] Brigitte Pansu,[d] and Guillaume Viau.[a,c]*

a. Université de Toulouse, INSA, UPS, LPCNO (Laboratoire de Physique et Chimie des Nano-Objets), F-31077 Toulouse, France; CNRS; UMR 5215 ; LPCNO, F-31077 Toulouse, France

lmlacroi@insa-toulouse.fr; phone +33561559652, fax +33561559697

b. Laboratoire National des Champs Magnétiques Intenses, CNRS-INSA-UJF-UPS, UPR3228; 143 Avenue de Rangueil, F-31400 Toulouse, France

c. Transpyrenean Advanced Laboratory for Electron Microscopy (TALEM), INSA - INA, CNRS - Universidad de Zaragoza, 30155 Toulouse, France

d. Laboratoire de Physique de Solides, UMR 8502, Bat. 510, Université Paris-Sud, F-91405 Orsay, France

e. Laboratorio de Microscopias Avanzadas (LMA), Instituto de Nanociencia de Aragon (INA), U. Zaragoza, C/ Mariano Esquillor s/n, 50018 Zaragoza (Spain).

f. Fundacion ARAID, 50004 Zaragoza, Spain.

Abstract

Ultrathin Au nanowires were prepared following two routes: the reduction of the lamellar phase [OY-Au^{I}Cl] in an excess of pure oleylamine and the direct reduction of Au^{III} in a solution of oleylamine in hexane. The superiority of the reduction of chloride gold precursor in isotropic environment is evidenced by SAXS measurements. A reaction yield of 75% is observed, an order of magnitude higher than the route involving the lamellar phase. Based on a detailed SAXS analysis, the soft template role of the [OY-Au^{I}Cl] intermediate solid phase was discarded for the nanowire growth. In the case of the liquid phase synthesis, DFT calculations evidence a cooperative adsorption and organisation of ions pairs at the surface of the ultrathin Au NWs. We propose that this charged backbone plays a key role in the unique growth mechanism of such anisotropic objects.

KEYWORDS: SAXS, lamellar phase, reaction yield, AuCl-oleylamine precursor, gold nanowires

1. Introduction

Ultrathin gold nanowires (Au NWs), exhibiting sub-2 nm diameter and micrometric length, have attracted expanding interests due to their unique properties, as high surface-to-volume ratio, mechanical flexibility and remarkable conductivity properties.[1,2] These features open the perspective towards various applications including electrical sensors,[3,4] fuel cell anodes,[5] elastic coiled springs,[6,7] or transparent electrodes.[8,9] To be competitive with the existing technologies, the developed alternatives should rely on cost-effective synthesis of Au NWs, i.e. with high yield and limited post-treatment requirements. Since the pioneer work of Halder and Ravishankar in 2007,[10] two main routes have been followed to synthesize these Au NWs: the first one involves the precipitation of an intermediate solid phase assuming that it acts as a soft-template for the wire growth,[11,12,13,14,15] while the second one is a direct reaction in an isotropic solution.[10,16,17,18] These two approaches led to the production of ultrathin Au NWs along with other nanoparticles such as spheres or rods. The quantitative analysis of the different populations of such nanostructures, and therefore the Au NWs yield estimation, even if it is crucial, cannot be easily addressed. Such problematic is far more generic than the Au NWs' synthesis. Indeed, physical properties such as plasmonic resonances, magnetism or luminescence, drastically depend on the size and the shape of nanoparticles. Though efficient separation techniques, such as centrifugation processes, are often used to narrow the size distribution of the nanoparticles obtained, size selection cannot be always applied. For instance, fragile objects or interacting particles cannot be easily sorted. Therefore, one should be able to assess, in a polymorphic synthesis, the yield of the desired objects. If transmission electron microscopy (TEM) is the technique of choice to deeply characterize the particle shape/size/composition, reliable estimation of the relative yield cannot be satisfactorily obtained due to sampling issues. Other techniques such as NMR and UV-visible spectroscopies, or dynamic light scattering can be used in specific cases to characterize nanostructures. However they cannot address the problematic of quantifying the relative yield of Au nanospheres and NWs due to the peculiar features of ultrathin NWs. Small Angle X-Ray Scattering (SAXS) is a state-of-art *in situ* technique which can shed light on the growth mechanism,[19,20,21] and the synthesis yield of metallic nanoparticles.[22,23] The quantitative analysis of SAXS data on an absolute scale enables to determine the number of particles along with their size and shape. In the case of monodisperse nanoparticles, SAXS analysis is fairly straightforward,[24] but for more complex populations, the interpretation becomes non univocal due to the averaging of several scattering profiles.[25,26] Coupled TEM and SAXS characterizations enable to obtain unambiguously quantitative analysis even on polymorphic nanoparticles.[27,28] We previously studied the growth of ultrathin Au nanowires in hexane medium coupling these two techniques and could extract a reaction yield for both, the side products nanoparticles and the nanowires of interest.[22] We report here a quantitative comparison between the two main routes for ultrathin Au NWs synthesis. The lamellar phase of the first approach is carefully analysed by structural, spectroscopic and computational techniques, confirming the formation of linear Au^I complexes. However, its prevalence as driving force towards unidimensional growth is questioned. Indeed, we clearly demonstrate the advantage of the liquid phase approach for a high yield synthesis of ultrathin Au NWs. Based on DFT calculations, we propose that a cooperative adsorption and organisation of ligands favors the stabilisation of such unique anisotropic objects.

2. Experimental section

2.1. Route 1: Soft-templating synthesis

Ultrathin Au NWs were prepared according to a slightly modified 2 steps procedure, described in the literature.[12]

Step 1: *synthesis of the [OY-Au^ICl] lamellar phase*. A 10 mM solution of gold was prepared: 20 mg of $HAuCl_4$,$3H_2O$ were dissolved in 5 mL oleylamine (OY, with a molar ratio OY/Au = 300) under ultrasonication (15 min). The solution was then kept undisturbed at 25°C for 48 h, leading to the formation of a white precipitate.

Step 2: *reduction of the [OY-Au^ICl] phase*. The white precipitate was separated from the yellow supernatant by centrifugation (2000 rpm, 2 min) and let to react 48 h at 45°C. A pink shade was progressively observed with time. The particles were separated from the excess oleylamine by a classical washing with mixed solvents (1:3) of toluene and ethanol. The obtained solution was centrifuged 10 min at 3500 rpm. The process was repeated 3 times. The final particles were redispersed in toluene.

2.2. Route 2: Liquid phase synthesis

The ultrathin gold nanowires (NWs) were prepared following a synthesis previously described.[16,22] Typically, 10 mM solution of gold was prepared: 40 mg of $HAuCl_4,3H_2O$ were dissolved in a solution containing 1.32 mL of oleylamine (OY, 400 mM, molar ratio OY/Au = 40) in 6.60 mL of hexane. 2.05 mL of triisopropylsilane (TIPS, 1M, molar ratio TIPS/Au = 100) were added to initiate the gold reduction. The solution was then kept undisturbed at 40°C for 3 hours. The particles were centrifuged once with ethanol (4000 rpm, 5 min) to remove the excess of reactants (OY, TIPS) and redispersed in hexane.

2.3. Characterization

The two syntheses of ultrathin gold nanowires were followed *in situ* by small angle X-Ray scattering (SAXS) and *ex situ* by transmission electron microscope (TEM). TEM images were obtained with a JEOL-1011F microscope, operating at 100 kV. HRTEM images were obtained using an imaging-side aberration-corrected FEI Titan-Cube microscope working at 80 kV, equipped with a Cs corrector (CESCOR from CEOS GmbH). The TEM samples were prepared by dispersing and depositing the raw synthesis products on a standard copper TEM grid coated with a thin amorphous carbon film. In situ SAXS measurements were performed on glass sealed capillaries (1.5 mm in diameter) containing either the white precipitate (route 1) or the hexane solution (route 2). The capillaries were heated 64 hours at 45°C (route 1) and 3 hours at 40°C (route 2). The SAXS data were expressed in terms of the scattering vector modulus $q = \frac{4\pi}{\lambda} sin(\theta)$, with λ the wavelength of the X-rays and θ the Bragg scattering angle. The experiments were performed for the soft-templating synthesis (route 1) at the LPS using a monochromatic X-ray beam generated by a rotating anode X-ray source (Cu Kα, 50 kV, 50 mA). The instrument covered a range of scattering vectors q between 0.01 and 0.18 $Å^{-1}$. For the liquid phase synthesis (route 2), the experiments were performed on the SWING beamline at the SOLEIL synchrotron using a monochromatic X-ray beam

(10 keV). The accessible q-range was between 6×10^{-3} and 0.6 $Å^{-1}$. For both instruments, the SAXS intensity was recorded on a CCD bi-dimensional detector placed inside a vacuum tube to reduce background. For background subtraction, the signal of a capillary filled with hexane was used. The SAXS intensities were normalized in absolute units (cm^{-1}) using the signal of a capillary filled with water as a standard. This allowed quantifying the volume fractions in solution of the spheres and the nanowires from the modeling results, as recently shown in a previous publication.[22] This method gives accurate values, and is based on the scattering contrast between gold and the organic solvent or the oleylamine (ρ_{gold} = 4650 e/nm^3, ρ_{hexane} = 230 e/nm^3, $\rho_{oleylamine}$ = 278 e/nm3, leading to a scattering contrast = ρ_{gold} - $\rho_{solvant}$ = 4400±50 e/nm^3 in both cases). Indeed, SAXS is sensitive only to the contrast between gold and the organic matter around (solvent and organic ligands). The volume fraction (vol_{frac}) is related to the gold cores of the nanoparticles, and it is defined by $Vol_{frac} = N\frac{V_p}{V}$, with V_P the particle's volume (gold core only), N the total number of particles and V the sample volume.

Wide Angle X-ray Scattering (WAXS) measurements (precipitate analysis) were performed at the LPS using a rotating anode X-ray source (Cu Kα, 40 kV, 40 mA) equipped with a MAR Image-Plate detector covering a range of scattering vectors q between 0.2 and 3.5 $Å^{-1}$.

2.4. Density Functional Theory calculations

All molecular calculations have been performed using the Gaussian09 suite of programs.[29] Geometry optimizations and subsequent electronic properties calculations have been carried out in the framework of density functional theory (DFT), using the B3PW91 hybrid functional.[30,31,32,33,34,35,36] A double-ζ basis set augmented by a set of polarization functions, namely the standard Pople's 6-31G(*d*,*p*) basis set, has been employed for H, C and N atoms.[37] Relativistic effective core potentials developed by the Stuttgart/Cologne groups and their associated basis sets[38] have been used for Au[39] and Cl.[40] This basis set was augmented with a set of *d*- or *f*-polarization functions for Au and Cl atoms (Au: ξ_f=1.0 ; Cl: ξ_f=0.643[41]). The nature of each stationary points was characterized by Hessian calculations whereas Gibbs free energies $G°$ at 298 K were calculated by means of the harmonic frequencies, *i.e.* by a straightforward application of statistical thermodynamic equations.[42]

The electronic properties of [111] oriented bulk Au NWs were calculated within the framework of the DFT considering periodic boundary conditions and the spin unpolarized or polarized constraint, depending of the system under study. These [111] direction oriented Au NWs, were generated by cleaving fcc bulk Au with low index surfaces, similarly to Roy et al.[43]. The exchange-correlation potential was approximated by the generalized gradient approach proposed by Perdew, Burke, and Ernzerhof (PBE).[44] Calculation of the energetic parameters as well as the geometry optimizations were carried out using the projector augmented waves (PAW) full-potential reconstruction[45,46] implemented in the Vienna *ab initio* simulation package, VASP.[47,48] To minimize errors arising from the frozen core approximation, we used the PAW data sets treating the 4p, 4d and 5s Ru states (14 valence electrons). A kinetic energy cut-off of 525 eV was sufficient to achieve a total energy convergence within several millielectronvolts for H adsorption. Van der Waals interactions were taken into consideration by adding a pairwise interatomic term E_{disp} to the Kohn−Shan DFT energies, which was evaluated using the revised DFT-D3 method of Grimme with Becke-Jonson damping.[49,50] For the geometry optimizations, a (1×1×5) Γ-centered[51] *k*-points grid was used to sample the reciprocal space combined with a Gaussian smearing of 0.02 eV width for the partial occupancies. Atoms were free to move until the residual forces on any direction were less than 0.02 eV/Å. The supercell size along the **a** and **b** directions was set to ensure a vacuum space of *ca.* 14 Å between periodic images of decorated Au NWs. Oleylamine and oleylammonium were replaced with methylamine and methylammonium for the sake of computational feasibility.

3. Results and Discussion

3.1. Comparative TEM study of the two approaches

Ultrathin Au nanowires were prepared following the two approaches reported in the literature: the method assuming a soft-templating role of the solid intermediate phase [OY-Au^{I}Cl] (route 1) based on a 2 steps reaction, and the liquid phase synthesis (route 2) relying on a direct reduction of $HAuCl_4$ in hexane (Scheme 1).

The particles were purified in both cases by precipitation in ethanol combined with a smooth centrifugation. Once the excess of ligands was removed, Au nanoparticles were redispersed in adequate solvent and deposited on TEM grids. Figure 1 shows comparative TEM images. The two syntheses yielded micrometric long Au nanowires, highly crystalline (Figure S1),[52] concomitantly with Au spheres, with diameters varying from ca. 8 nm for the soft-templating approach (route 1, Figure 1a) to ca. 1.5 nm for the liquid phase synthesis (route 2, Figure 1b). Apart from this difference in the diameter of side products, TEM characterizations do not allow to conclude on the quantity of nanowires for these two reactions. Therefore, deeper analyses were undertaken to obtain quantitative elements to compare both approaches. The reaction yield (expressed in %) for one type of nanoparticles (spheres or nanowires) was defined as the ratio between the amount of gold atoms inside this type of nanoparticles and the total amount of gold atoms in presence.

3.2. Analysis of the soft-templating approach

The reduction of the gold chloride salt (here $HAuCl_4$) was performed in pure oleylamine in a two steps process (Scheme 1). In step 1, after 48 h of reaction at room temperature, a white precipitate was obtained and separated by centrifugation. In step 2, this precipitate was placed at 45°C, ultrathin Au NWs and polydisperse nanospheres were formed upon time. These two steps have been quantitatively studied to estimate the resulting global Au NWs yield.

Step 1. Analysis of the precipitate

Since this precipitate plays the role of precursor for the second step, further characterizations of the isolated precipitate were undertaken. TEM energy dispersive X-Ray spectroscopy (EDS) indicated the presence of Au and Cl ions in a 1 to 1 ratio (Figure S2), in agreement with the AuCl-oleylamine complex proposed previously.[12,18] However, both thermogravimetric (TGA) and differential scanning calorimetry (DSC) analysis revealed a gold content of solely 2% in mass (Figure S3), far from the 40% expected in case of pure AuCl-oleylamine. Therefore, free OY molecules precipitated with the the [OY-Au^{I}Cl] solid phase.

The structural characterization of the precipitate was performed using WAXS (Wide Angle X-ray Scattering). First, WAXS pattern (Figure 2a) revealed an amorphous peak around q = 1.4 $Å^{-1}$ plus some weak narrow peaks at even higher scattering vectors. Thus, coexistence of two states were evidenced for the organic chains of the oleylamine molecules. Though most of oleylamine molecules were in a molten state (amorphous peak), as in liquid pure oleylamine, some were crystallised (weak narrow peaks). Moreover, at smaller scattering vectors, a series of intense diffraction peaks, consistent with (00l) peaks of a lamellar phase, was observed (Figure 2a). An interlamellar distance of 4.8 nm could be determined from the indexation of these peaks. The length of fully extended oleylamine being of 2.0 nm,[53] the lamellar structure could be composed of Au planes separated by two molecules of oleylamine partly interdigitated (Figure 2b). This model was confirmed by further experiments where the alkyl chain length of the amine was decreased from 12 carbons down to 4 (Figure S4). The interlamellar distance varied linearly with the number of atoms of the alkyl chain. The corresponding linear fit confirmed the presence of two molecules partly interdigitated and evidenced Au planes of ca. 0.6 nm (Figure S5).

DFT calculations were performed to address the stable configuration of AuCl-amine precursor within the lamellar phase. The precursor adopted a linear configuration as evidenced in Figure 3. Aurophilic bounds, as long as hydrogen bounding between successive Cl and NH_2 groups, stabilized this one-dimensional organisation, which could play a decisive role in the future growth of ultrathin Au NWs.

The formation of this lamellar phase, composed of the linear Cl-Au^I- RNH_2 precursor, was not total. Indeed, all the Au initially introduced was not retained in the precipitate because a large fraction was lost in the supernatant. The quantification of the total mass of the precipitate (typically 300 mg) and the mass fraction of Au (2%) revealed a 60% yield for step 1 (Scheme 1).

Step 2 : reduction of Au^I precursor into Au^0

Step 2 consisted in the final reduction of the Au^I precursor previously obtained into Au nanoparticles. We studied the effect of temperature on this reduction step by in-situ SAXS and ex-situ TEM. At room temperature, the initial precipitate gave a diffraction peak at a scattering vector q = 0.13 $Å^{-1}$, corresponding to the (001) peak of the lamellar phase previously described (Figure 2) and a concomitant q^{-4} power law at small q vectors (SAXS experiment) (Figure 4a). This q^{-4} signal, known as Porod contribution, arisen form the scattering at the interface between the lamellar phase domains and the surrounding oleylamine. This two features, (001) diffraction peak and Porod contribution, attested the presence of the lamellar phase during the reaction. With time, this initial signal evolved, allowing following the growth of gold nanoparticles. The adjustment of the experimental curve gave access to the size and shape of the objects along with their volume fraction. Compared to the theoretic 8.5×10^{-4} volume fraction of gold deduced from TGA, the reaction yield after step 2 could thus be deduced.

Below 45°C, the reaction kinetic was very slow (Figure 4b). The modification of the scattering profile with time was fairly weak, leading to a difficult analysis of the nanoparticle populations. Even after 70 h of reaction, a yield of only 0.6% was determined. Between 45 and 50°C, the reaction was faster (Figure 4c and S6a). The fitting of the scattering profile at different reaction time evidenced at first the growth of Au NWs, then followed by the growth of Au nanospheres (Figure S7). After 48h of reaction, TEM images confirmed the presence of both populations (Figure 5a). While the nanospheres' volume fraction increased continuously with time, Au NWs' one saturated after 30 h at 3×10^{-5} (Figure 6).

Increasing the reaction temperature above 50°C led to the melting of the lamellar phase (Figure 4d and S6b), as revealed by the disappearance of the (001) peak and the Porod contribution. Under such conditions, only polydisperse spheres were detected both by SAXS and TEM (Figure 5b). Their diameters increased from 5 to 7 nm during the first 30 h, in agreement with the size distribution determined from TEM image (Figure S8). After that, the particles tended to form aggregates as evidenced by the additional correlation peak observed by SAXS. From the fit of this correlation peak, using the Percus-Yevick expression of the structure factor for hard spheres, one could deduce that, after 45 h, the spheres were all embedded in these agglomerates. The position of the correlation peak was related to the average distance between the spheres, and the typical separation distance in-between two gold-cores was found equal to 3.5 ± 1.7 nm (Figure S9).

Optimization of the Au NWs synthesis

Regarding the mastery of the soft-templating approach for the quantitative synthesis of Au NWs, the nanowires yields were fairly low and did not exceed 3% for the whole process. This low yield resulted from i) the chemical equilibrium between Au^{I} and Au^{III} which led to a 40% loss of gold after step 1, ii) the insignificant reduction of Au^{I} to Au^{0} during step 2, which did not further evolve with time.

To improve the total yield of the soft-templating reaction, we tried to optimize these two drawbacks. Step 1 was performed at higher temperature and/or for longer time. However, neither of these parameters led to a quantitative modification of the chemical equilibrium. They both favour the reduction of Au^{I} into Au^{0}, blurring the demarcation between step 1 and step 2. For instance, after 25 days at room temperature, Au NWs and spheres could be observed concomitantly with Au^{III} as evidenced by the characteristic yellow colour of the supernatant (Figure S10).

Regarding the reduction Au^{I} to Au^{0}, neither the temperature, nor the reaction time could favour a quantitative step 2 reaction. In both cases, reduction yield below 10% were obtained, and Au nanospheres were formed detrimentally to Au NWs. Therefore, stronger reducing agents such as H_2 or triisopropylsilane (TIPS), which was used as reducing agent in the liquid phase synthesis, were added during step 2. None of them led to the quantitative formation of Au nanowires. A 3 bars H_2 atmosphere fastened the reaction and yielded spherical and rod like NPs, while TIPS did not drastically affect the kinetic, leading to similar particles as the ones obtained in presence of oleylamine solely (Figure S11). Thus, the synthesis of Au NWs following the soft-templating approach (route 1) may not be strictly limited by the reduction of the lamellar phase, as evidenced by the experiments in presence of stronger reducing agent, but more likely by the diffusion within the soft-template.

3.3. Route 2 : Liquid phase synthesis

This synthesis approach relied on a one step liquid phase reaction, where the gold chloride salt was solubilised in hexane in presence of oleylamine and reduced by triisopropylsilane. We followed the growth of Au NWs by in-situ SAXS and could characterize a reaction yield for Au NWs, which should be compared to the global yield obtained for the soft-templating approach. The scattering profiles could be fairly easily adjusted by summing only the contributions of spheres and wires, no diffraction peak neither Porod contribution did hinder the signals. Small spheres of 1.7 nm of diameter were present since the beginning of the reaction, as evidenced by the characteristic plateau in the scattering profile. Then, a q^{-1} contribution, characteristics of Au NWs, appeared and grew with time. The volume fractions of both populations were deduced from the fitting parameters.[22] The diameter of the nanowires was found constant at 1.7 nm with a polydispersity on the diameter distribution of only 2%. The reduction Au^{III} – Au^{0} was total after only 90 min of reaction at 40°C, the yield of Au NWs being of 75%, far above the 3% obtained with the route 1 (Figure 7).

3.4. Discussion

The soft-templating approach is based on the assumption that the lamellar phase plays a key role in the growth of Au NWs. Indeed, the in situ SAXS study of the route 1 shows that Au NWs are indeed obtained in presence of this lamellar phase. Moreover, for reaction temperature above 50°C, the lamellar phase melt and only spherical particles are obtained instead. Therefore, at first sight, our experiments seem to confirm the importance of the lamellar phase. However, the growth of Au NWs within the lamellar phase should have modified the XRD pattern through an increasing of the inter-lamellar distance, the 1.7 nm diameter of the Au NWs being much larger than the initial thickness of the Au plans, and/or a broadening of the (00l) lines due to a loss of crystallographic correlations. Neither the position nor the broadening of the (001) peak of the lamellar phase showed any modification during the appearance of the NWs, thus the growth may not directly occurred within the lamellar phase. Moreover, the reduction of the Au precursor is hindered in presence of the lamellar phase, leading to a final Au NWs yield below 3%. On the contrary, liquid phase reaction led to a quantitative reduction and a 75% yield. Thus, we conclude that the Au NWs growth does not take place inside a soft lamellar template, as previously assumed. The lamellar phase is actually detrimental to the growth, as revealed by the low reaction yield.

If the growth within a lamellar phase acting as a soft template was an elegant way to explain the unique growth of Au ultrathin nanowires, new hypotheses on such anisotropic driving force should now be invoked. Oriented attachment of preformed spherical particles was previously discarded due to the fairly constant spheres' volume fraction evidenced by SAXS.[22] The growth may therefore occur in preformed cylindrical micelles,[54] or thanks to a cooperative effect between surfactants organisation and Au reduction, previously described as a "zip" mechanism for the growth of Au nanorods in water.[55] DFT calculations of the energetic stabilisation by polar heads (oleylamine vs. oleylammonium chloride) were performed to investigate these hypotheses. Due to computational limitation, the alkyl chain was limited to one carbon. Methylamine adsorbs preferentially on top of the gold surface atom with the lowest coordination number (c.n.: 5). Its adsorption energy, -22.4 kcal/mol, was roughly twice as strong as on the close-packed Au(111) surface. Actually this value is in fair agreement with the adsorption energy on a gold adatom (c.n : 3) [56] placed in the fcc position of this surface (see Table S1 and ref 55). The methylammonium chloride ion pair, with polar ammonium head lying above an adsorbed chloride, bound similarly to methylamine at the Au NW surface, with almost the same adsorption energy (-19.1 kcal/mol). Despite the low coordination number of gold surface atoms and possible finite-size effects,[57] these values remain quite low. Nevertheless, the methylammonium chloride ion pair adsorption was significantly enhanced if both moieties were simultaneously adsorbed on the surface (Figure S12). Such adsorption, when occurring along the nanowire, makes an alternant positive/negative pattern that enhances adsorption strength. Figure 8 shows the stabilisation with six methylammonium chloride entities per unit cell. The resulting adsorption energy was found to be -37.7 kcal/mol per ion pair, suggesting that a network of ion pairs could stabilize the surface of the nanowire. Thus, these preliminary DFT results tend to show that a "zip" mechanism may also be invoked in the case of ultrathin Au NWs in non polar solvent.

4. Conclusion

Ultrathin Au nanowires were prepared following two routes: the reduction of the lamellar phase [OY-Au^{I}Cl] in an excess of pure oleylamine and the direct reduction of Au^{III} in a solution of oleylamine in hexane. In both cases nanospheres were found as side product. SAXS analyses enabled to determine with a good precision the volume fraction of the different gold particles present in solution, from which reaction yields were inferred. The superiority of the reduction of gold chloride precursor in isotropic environment was clearly evidenced. A large reaction yield of 75% was determined, an order of magnitude higher than the route involving the lamellar phase. We demonstrated that neither the reaction temperature/time nor the addition of stronger reducing agent could improve the Au NWs yield in presence of the lamellar phase. Indeed, after 30 h of reaction and for temperature above 50°C, only polydisperse Au NPs were obtained. This study allows ruling out the assumption that the [OY-Au^{I}Cl] intermediate solid phase acts as a soft template for the nanowire growth. In the case of the liquid phase synthesis, DFT calculations evidenced a cooperative adsorption and organisation of ions pairs at the surface of the ultrathin Au NWs. We propose that such charged backbone plays a key role in the unique growth mechanism of such anisotropic objects.

ACKNOWLEDGMENT

The authors acknowledge the financial support of the Midi-Pyrénées region, of the university of Toulouse, PRES, of the Labex NEXT, N° 11 LABX 075, of the French GDR Or-Nano. Simon Cayez (LPCNO, Toulouse) is warmly thanked for the EDS analysis and the preparation of TEM grids. We thank Francis Chouzenoux (LPCNO, Toulouse) for TGA-DSC measurements. R.A. acknowledges funding from the Spanish Ministerio de Economia y Competitividad (FIS2013-46159-C3-3-P). Microscopy work was conducted in the Unité Mixte de Service Castaing, Toulouse (France) and in the Laboratorio de Microscopias Avanzadas at the Instituto de Nanociencia de

Aragon, Universidad de Zaragoza (Spain). The research leading to these results has received funding from the European Union Seventh Framework Program under Grant Agreement 312483 - ESTEEM2 (Integrated Infrastructure Initiative − I3). RP thanks the HPCs CALcul en MIdi-Pyrénées (CALMIP-Hyperion and CALMIP-EOS, grant P0611) and the Grand Equipement National de Calcul Intensif (GENCI-TGCC-Curie, grant 6211) for generous allocations of computer time.

ASSOCIATED CONTENT

Supporting Information. Additional SAXS diagrams, TEM and HRTEM images. TEM-EDS, TGA and DSC analysis of the precipitate. XRD patterns of the precipitate obtained with different amines and the evolution of the corresponding interplanar distance. This material is available free of charge via the Internet at http://pubs.acs.org.

AUTHOR INFORMATION

Corresponding Author

* lmlacroi@insa-toulouse.fr; phone +33561559652, fax +33561559697

Author Contributions

The manuscript was written through contributions of all authors. A.L., L.-M.L, A.R. and G.V. performed the chemical synthesis. R.A. performed HRTEM study. A.L., M.I.C and B.P. performed and analyzed SAXS measurements. L.M. and R.P. performed DFT calculations.

Funding Sources

The authors acknowledge the financial support of the Midi-Pyrénées region, of the university of Toulouse, PRES, of the Labex NEXT, N° 11 LABX 075, of the French GDR Or-Nano, of the European Union Seventh Framework Program under Grant Agreement 312483 - ESTEEM2.

REFERENCES

(1) Loubat, A.; Escoffier, W.; Lacroix, L.-M.; Viau, G.; Tan, R.; Carrey, J.; Warot-Fonrose, B.; Raquet, B. Cotunneling Transport in Ultra-Narrow Gold Nanowire Bundles. *Nano Res.* **2013**, *6*, 644–651.

(2) Pud, S.; Kisner, A.; Heggen, M.; Belaineh, D.; Temirov, R.; Simon, U.; Offenhäusser, A.; Mourzina, Y.; Vitusevich, S. Features of Transport in Ultrathin Gold Nanowire Structures. *Small* **2013**, *9*, 846–852.

(3) Cui, H.; Hong, C.; Ying, A.; Yang, X.; Ren, S. Ultrathin Gold Nanowire-Functionalized Carbon Nanotubes for Hybrid Molecular Sensing. *ACS Nano* **2013**, *7*, 7805–7811.

(4) Kisner, A.; Heggen, M.; Mayer, D.; Simon, U.; Offenhäusser, A.; Mourzina, Y. Probing the Effect of Surface Chemistry on the Electrical Properties of Ultrathin Gold Nanowire Sensors. *Nanoscale* **2014**, *6*, 5146.

(5) Yang, L.; Zhang, Y.; Chu, M.; Deng, W.; Tan, Y.; Ma, M.; Su, X.; Xie, Q.; Yao, S. Facile Fabrication of Network Film Electrodes with Ultrathin Au Nanowires for Nonenzymatic Glucose Sensing and glucose/O2 Fuel Cell. *Biosens. Bioelectron.* **2014**, *52*, 105–110.

(6) Xu, J.; Wang, H.; Liu, C.; Yang, Y.; Chen, T.; Wang, Y.; Wang, F.; Liu, X.; Xing, B.; Chen, H. Mechanical Nanosprings: Induced Coiling and Uncoiling of Ultrathin Au Nanowires. *J. Am. Chem. Soc.* **2010**, *132*, 11920–11922.

(7) Xu, J.; Jiang, W. Confinement of Polymer-Tethered Gold Nanowires in Polymeric Colloids. *Macromolecules* **2014**, *47*, 2396–2403.

(8) Chen, Y.; Ouyang, Z.; Gu, M.; Cheng, W. Mechanically Strong, Optically Transparent, Giant Metal Superlattice Nanomembranes From Ultrathin Gold Nanowires. *Adv. Mater.* **2013**, *25*, 80–85.

(9) Sánchez-Iglesias, A.; Rivas-Murias, B.; Grzelczak, M.; Pérez-Juste, J.; Liz-Marzán, L. M.; Rivadulla, F.; Correa-Duarte, M. A. Highly Transparent and Conductive Films of Densely Aligned Ultrathin Au Nanowire Monolayers. *Nano Lett.* **2012**, *12*, 6066–6070.

(10) Halder, A.; Ravishankar, N. Ultrafine Single-Crystalline Gold Nanowire Arrays by Oriented Attachment. *Adv. Mater.* **2007**, *19*, 1854–1858.

(11) Lu, X.; Yavuz, M. S.; Tuan, H.-Y.; Korgel, B. A.; Xia, Y. Ultrathin Gold Nanowires Can Be Obtained by Reducing Polymeric Strands of Oleylamine−AuCl Complexes Formed via Aurophilic Interaction. *J. Am. Chem. Soc.* **2008**, *130*, 8900–8901.

(12) Huo, Z.; Tsung, C.; Huang, W.; Zhang, X.; Yang, P. Sub-Two Nanometer Single Crystal Au Nanowires. *Nano Lett.* **2008**, *8*, 2041–2044.

(13) Kura, H.; Ogawa, T. Synthesis and Growth Mechanism of Long Ultrafine Gold Nanowires with Uniform Diameter. *J. Appl. Phys.* **2010**, *107*, 074310.

(14) Kisner, A.; Heggen, M.; Fernández, E.; Lenk, S.; Mayer, D.; Simon, U.; Offenhäusser, A.; Mourzina, Y. The Role of Oxidative Etching in the Synthesis of Ultrathin Single-Crystalline Au Nanowires. *Chem. - Eur. J.* **2011**, *17*, 9503–9507.

(15) Imura, Y.; Tanuma, H.; Sugimoto, H.; Ito, R.; Hojo, S.; Endo, H.; Morita, C.; Kawai, T. Water-Dispersible Ultrathin Au Nanowires Prepared Using a Lamellar Template of a Long-Chain Amidoamine Derivative. *Chem. Commun.* **2011**, *47*, 6380.

(16) Feng, H.; Yang, Y.; You, Y.; Li, G.; Guo, J.; Yu, T.; Shen, Z.; Wu, T.; Xing, B. Simple and Rapid Synthesis of Ultrathin Gold Nanowires, Their Self-Assembly and Application in Surface-Enhanced Raman Scattering. *Chem. Commun.* **2009**, 1984.

(17) Kang, Y.; Ye, X.; Murray, C. B. Size- and Shape-Selective Synthesis of Metal Nanocrystals and Nanowires Using CO as a Reducing Agent. *Angew. Chem. Int. Ed.* **2010**, *49*, 6156–6159.

(18) Li, Z.; Tao, J.; Lu, X.; Zhu, Y.; Xia, Y. Facile Synthesis of Ultrathin Au Nanorods by Aging the AuCl(oleylamine) Complex with Amorphous Fe Nanoparticles in Chloroform. *Nano Lett.* **2008**, *8*, 3052–3055.

(19) Polte, J.; Erler, R.; Thünemann, A. F.; Sokolov, S.; Ahner, T. T.; Rademann, K.; Emmerling, F.; Kraehnert, R. Nucleation and Growth of Gold Nanoparticles Studied *via in Situ* Small Angle X-Ray Scattering at Millisecond Time Resolution. *ACS Nano* **2010**, *4*, 1076–1082.

(20) Wuithschick, M.; Paul, B.; Bienert, R.; Sarfraz, A.; Vainio, U.; Sztucki, M.; Kraehnert, R.; Strasser, P.; Rademann, K.; Emmerling, F.; et al. Size-Controlled Synthesis of Colloidal Silver Nanoparticles Based on Mechanistic Understanding. *Chem. Mater.* **2013**, *25*, 4679–4689.

(21) Abécassis, B.; Testard, F.; Spalla, O.; Barboux, P. Probing in Situ the Nucleation and Growth of Gold Nanoparticles by Small-Angle X-Ray Scattering. *Nano Lett.* **2007**, *7*, 1723–1727.

(22) Loubat, A.; Impéror-Clerc, M.; Pansu, B.; Meneau, F.; Raquet, B.; Viau, G.; Lacroix, L.-M. Growth and Self-Assembly of Ultrathin Au Nanowires into Expanded Hexagonal Superlattice Studied by in Situ SAXS. *Langmuir* **2014**, *30*, 4005–4012.

(23) Hubert, F.; Testard, F.; Thill, A.; Kong, Q.; Tache, O.; Spalla, O. Growth and Overgrowth of Concentrated Gold Nanorods: Time Resolved SAXS and XANES. *Cryst. Growth Des.* **2012**, *12*, 1548–1555.

(24) McKenzie, L. C.; Haben, P. M.; Kevan, S. D.; Hutchison, J. E. Determining Nanoparticle Size in Real Time by Small-Angle X-Ray Scattering in a Microscale Flow System. *J. Phys. Chem. C* **2010**, *114*, 22055–22063.

(25) Sun, Y.; Ren, Y. In Situ Synchrotron X-Ray Techniques for Real-Time Probing of Colloidal Nanoparticle Synthesis. *Part. Part. Syst. Charact.* **2013**, *30*, 399–419.

(26) Thünemann, A. F.; Kegel, J.; Polte, J.; Emmerling, F. Superparamagnetic Maghemite Nanorods: Analysis by Coupling Field-Flow Fractionation and Small-Angle X-Ray Scattering. *Anal. Chem.* **2008**, *80*, 5905–5911.

(27) Koerner, H.; MacCuspie, R. I.; Park, K.; Vaia, R. A. In Situ UV/Vis, SAXS, and TEM Study of Single-Phase Gold Nanoparticle Growth. *Chem. Mater.* **2012**, *24*, 981–995.

(28) Wang, W.; Zhang, K.; Cai, Q.; Mo, G.; Xing, X. Q.; Cheng, W. D.; Chen, Z. J.; Wu, Z. H. Real-Time SAXS and Ultraviolet-Visible Spectral Studies on Size and Shape Evolution of Gold Nanoparticles in Aqueous Solution. *Eur. Phys. J. B* **2010**, *76*, 301–307.

(29) Frisch, M. J.; Trucks, G. W.; Schlegel, H. B.; Scuseria, G. E.; Robb, M. A.; Cheeseman, J. R.; Scalmani, G.; Barone, V.; Mennucci, B.; Petersson, G. A., et al. Gaussian 09, Revision A.1; Gaussian, Inc.: Wallingford, CT, 2009.

(30) Becke, A. D. Density-Functional Thermochemistry. III. The Role of Exact Exchange. *J Chem Phys* **1993**, *98*, 5648–5652.

(31) Burke, K.; Perdew, J. P.; Wang, Y. Electronic Density Functional Theory: Recent Progress and New Directions. In; Dobson, J. F.; Vignale, G.; Das, M. P., Eds.; Plenum: New-York, 1998.

(32) Perdew, J. P. Electronic Structure of Solids. In; Ziesche, P.; Eschrig, H., Eds.; Akademie: Berlin, 1991.

(33) Perdew, J. P.; Chevary, J. A.; Vosko, S. H.; Jackson, K. A.; Pederson, M. R.; Singh, D. J.; Fiolhais, C. Atoms, Molecules, Solids, and Surfaces: Applications of the Generalized Gradient Approximation for Exchange and Correlation. *Phys Rev B* **1992**, *46*, 6671–6687.

(34) Perdew, J. P.; Chevary, J. A.; Vosko, S. H.; Jackson, K. A.; Pederson, M. R.; Singh, D. J.; Fiolhais, C. Erratum: Atoms, Molecules, Solids, and Surfaces: Applications of the Generalized Gradient Approximation for Exchange and Correlation. *Phys Rev B* **1993**, *48*, 4978.

(35) Perdew, J. P.; Burke, K.; Wang, Y. Generalized Gradient Approximation for the Exchange-Correlation Hole of a Many-Electron System. *Phys Rev B* **1996**, *54*, 16533–16539.

(36) Perdew, J. P.; Burke, K.; Wang, Y. Erratum: Generalized Gradient Approximation for the Exchange-Correlation Hole of a Many-Electron System. *Phys Rev B* **1998**, *57*, 14999.

(37) Hehre, W. J.; Ditchfield, R.; Pople, J. A. Self-Consistent Molecular Orbital Methods. XII. Further Extensions of Gaussian-Type Basis Sets for Use in Molecular Orbital Studies of Organic Molecules. *J Chem Phys* **1972**, *56*, 2257–2261.

(38) Effective core potentials and associated basis sets can be downloaded from: http://www.tc.uni-koeln.de/PP/clickpse.en.html

(39) Schwerdtfeger, P.; Dolg, M.; Schwarz, W. H. E.; Bowmaker, G. A.; Boyd, P. D. W. Relativistic Effects in Gold Chemistry. I. Diatomic Gold Compounds. *J Chem Phys* **1989**, *91*, 1762–1774.

(40) Bergner, A.; Dolg, M.; Küchle, W.; Stoll, H.; Preuß, H. Ab Initio Energy-Adjusted Pseudopotentials for Elements of Groups 13-17. *Mol Phys* **1993**, *80*, 1431–1441.

(41) Maron, L.; Teichteil, C. On the Accuracy of Averaged Relativistic Shape-Consistent Pseudopotentials. *Chem Phys* **1998**, *237*, 105–122.

(42) McQuarrie, D. A. *Statistical Mechanics*; 2nd ed.; University Science Books: Sausalito, California (USA), 2000.

(43) Roy, A.; Pandey, T.; Ravishankar, N.; Singh, A. K. Single Crystalline Ultrathin Gold Nanowires: Promising Nanoscale Interconnects. *AIP Adv.* **2013**, *3*, 032131.

(44) Perdew, J. P.; Burke, K.; Ernzerhof, M. Generalized Gradient Approximation Made Simple. *Phys Rev Lett* **1996**, *77*, 3865–3868.

(45) Blöchl, P. E. Projector Augmented-Wave Method. *Phys Rev B* **1994**, *50*, 17953–17979.

(46) Kresse, G.; Joubert, D. From Ultrasoft Pseudopotentials to the Projector Augmented-Wave Method. *Phys Rev B* **1999**, *59*, 1758–1775.

(47) Kresse, G.; Fürthmuller, J. Efficiency of Ab Initio Total Energy Calculations for Metals and Semiconductors Using a Plane-Wave Basis Set. *Comput Mater Sci* **1996**, *6*, 15–50.

(48) Kresse, G.; Fürthmuller, J. Efficient Iterative Schemes for Ab Initio Total-Energy Calculations Using a Plane-Wave Basis Set. *Phys Rev B* **1996**, *54*, 11169–11186.

(49) Grimme, S.; Antony, J.; Ehrlich, S.; Krieg, H. A Consistent and Accurate Ab Initio Parametrization of Density Functional Dispersion Correction (DFT-D) for the 94 Elements H-Pu. *J Chem Phys* **2010**, *132*, 154104.

(50) Grimme, S.; Ehrlich, S.; Goerigk, L. Effect of the Damping Function in Dispersion Corrected Density Functional Theory. *J Comput Chem* **2011**, *32*, 1456–1465.

(51) Monkhorst, H. J.; Pack, J. D. Special Points for Brillouin-Zone Integrations. *Phys Rev B* **1976**, *13*, 5188–5192.

(52) Lacroix, L.-M.; Arenal, R.; Viau, G. Dynamic HAADF-STEM Observation of a Single-Atom Chain as the Transient State of Gold Ultrathin Nanowire Breakdown. *J. Am. Chem. Soc.* **2014**.

(53) Mourdikoudis, S.; Liz-Marzán, L. M. Oleylamine in Nanoparticle Synthesis. *Chem. Mater.* **2013**, *25*, 1465–1476.

(54) Pazos-Pérez, N.; Baranov, D.; Irsen, S.; Hilgendorff, M.; Liz-Marzán, L. M.; Giersig, M. Synthesis of Flexible, Ultrathin Gold Nanowires in Organic Media. *Langmuir* **2008**, *24*, 9855–9860.

(55) Gao, J.; Bender, C. M.; Murphy, C. J. Dependence of the Gold Nanorod Aspect Ratio on the Nature of the Directing Surfactant in Aqueous Solution. *Langmuir* **2003**, *19*, 9065–9070.

(56) Hoft, R. C.; Ford, M. J.; McDonagh, A. M.; Cortie, M. B. Adsorption of Amine Compounds on the Au(111) Surface: A Density Functional Study. *J Phys Chem C* **2007**, *111*, 13886–13891.

(57) Kleis, J.; Greeley, J.; Romero, N. A.; Morozov, V. A.; Falsig, H.; Larsen, A. H.; Lu, J.; Mortensen, J. J.; Dulak, M.; Thygesen, K. S.; et al. Finite Size Effects in Chemical Bonding: From Small Clusters to Solids. *Catal Lett* **2011**, *141*, 1067–1071.

Figure captions

Scheme 1 : Overview of a) the soft-templating approach (route 1) based on a 2-step reaction. The step 2 uses only the white precipitate, obtained after removal of the supernatant. b) the liquid phase synthesis (route 2).

Figure 1. TEM images of Au nanoparticles obtained with a) the soft-templating approach (route 1) and b) the liquid phase synthesis (route 2).

Figure 2. a) XRD pattern of the precipitate obtained after step 1 (red) and the corresponding oleylamine reference (black). b) Schematic view of the lamellar phase with partly interdigitated alkyl chains.

Figure 3. DFT calculation of the stable configuration of Cl-Au^{I}-RNH_2 complexes. 3 carbons alkyl chain amines were considered due to computational time limitation. In green : Cl, blue : N, Grey : C, White : H, Black : Au^{I}.

Figure 4. SAXS pattern of a) starting precipitate at room temperature and its further evolution with time at b) 43°C, c) 48°C and d) 53°C.

Figure 5. TEM images of the particles obtained at a) 48°C after 45h and b) 53°C after 30 h with the soft templating approach (route 1).

Figure 6. Volume fraction of nanospheres (black squares), nanowires (red circles) and their sum (blue triangles) deduced from SAXS profiles fitting at 45°C.

Figure 7. Volume fractions calculated from the SAXS modelling at different times. Inset : Small angle X-ray scattering results measured at 40 °C from t=0 to t=150 min.

Figure 8. DFT geometry of a gold nanowire stabilized by methylammonium chloride (the unitcell is highlighted, as well as the faceting of the NW resulting from the low-index surface cleavage). In green: Cl, blue: N, grey: C, white: H, yellow: Au.

Figures

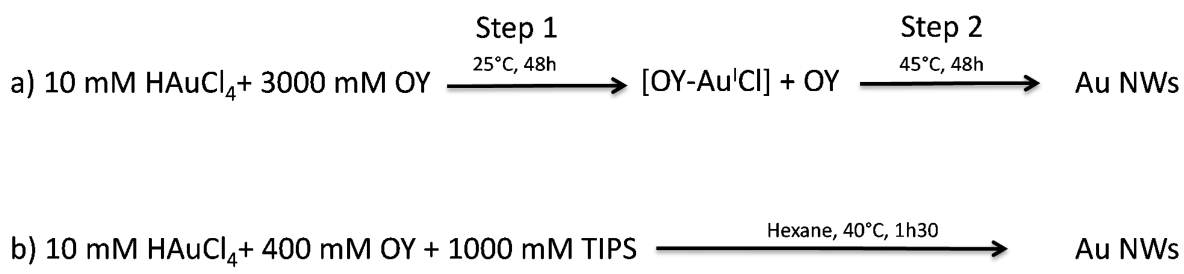

Scheme 1

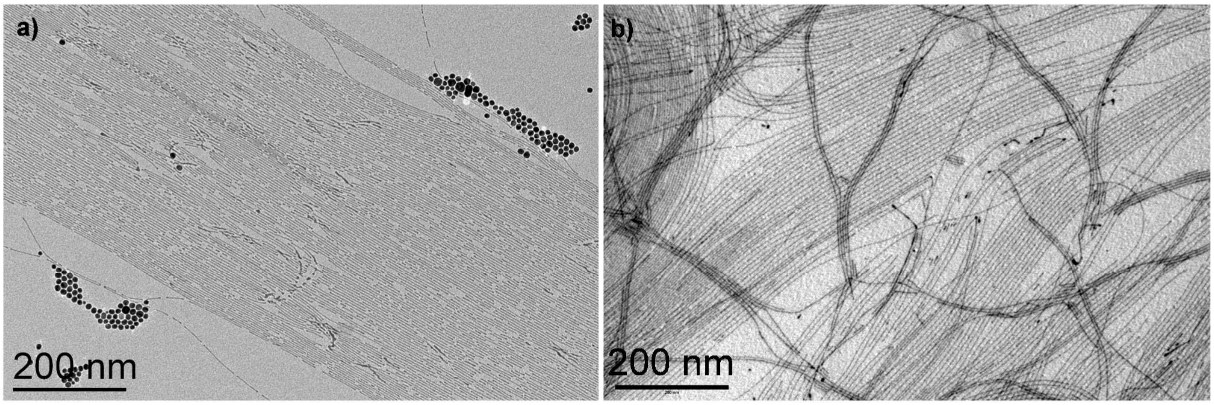

Figure 1

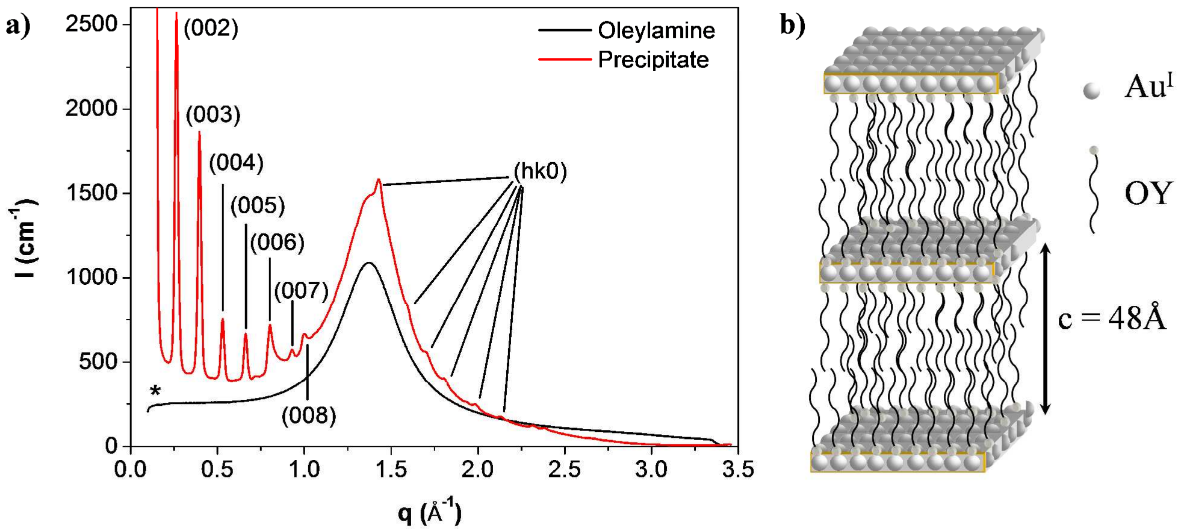
a)
b)
2500
2000
1500
1000
500
0
I (cm-1)
0.0
0.5
1.0
1.5
2.0
2.5
3.0
3.5
q (Å-1)
Oleylamine
Precipitate
(002)
(003)
(004)
(005)
(006)
(007)
(008)
(hk0)
*
AuI
OY
c = 48Å

Figure 2

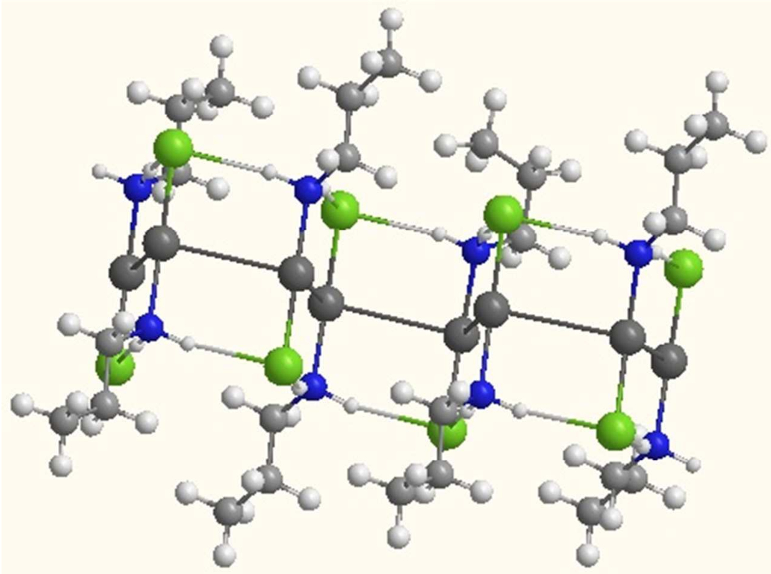

Figure 3.

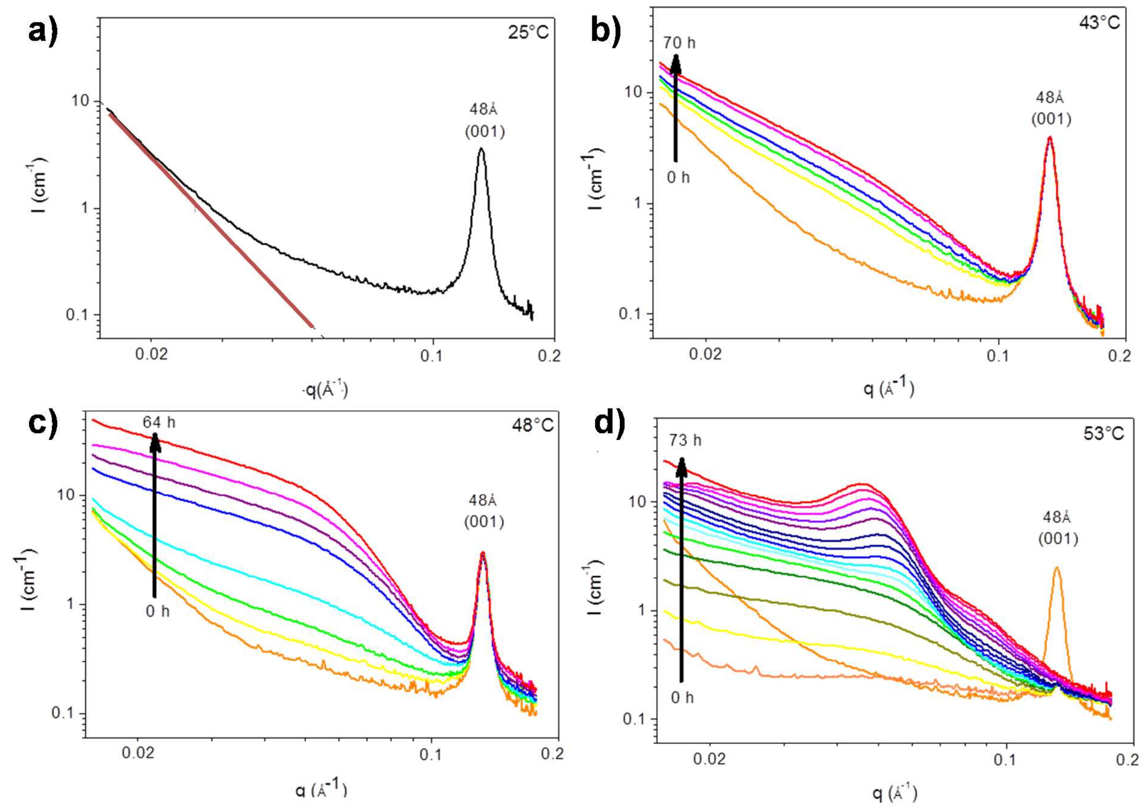
a)
25°C
48Å
(001)
I (cm^{-1})
q(Å^{-1})
b)
43°C
70 h
0 h
48Å
(001)
I (cm^{-1})
q (Å^{-1})
c)
48°C
64 h
0 h
48Å
(001)
I (cm^{-1})
q (Å^{-1})
d)
53°C
73 h
0 h
48Å
(001)
I (cm^{-1})
q (Å^{-1})

Figure 4

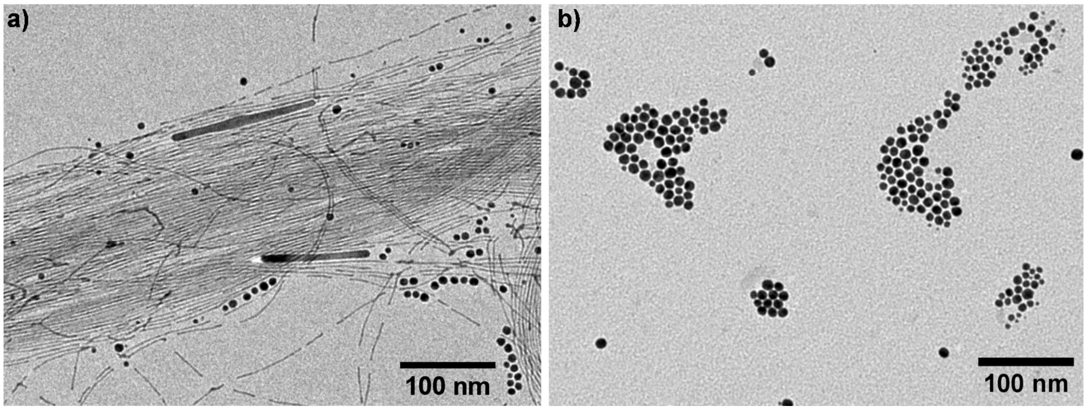

Figure 5

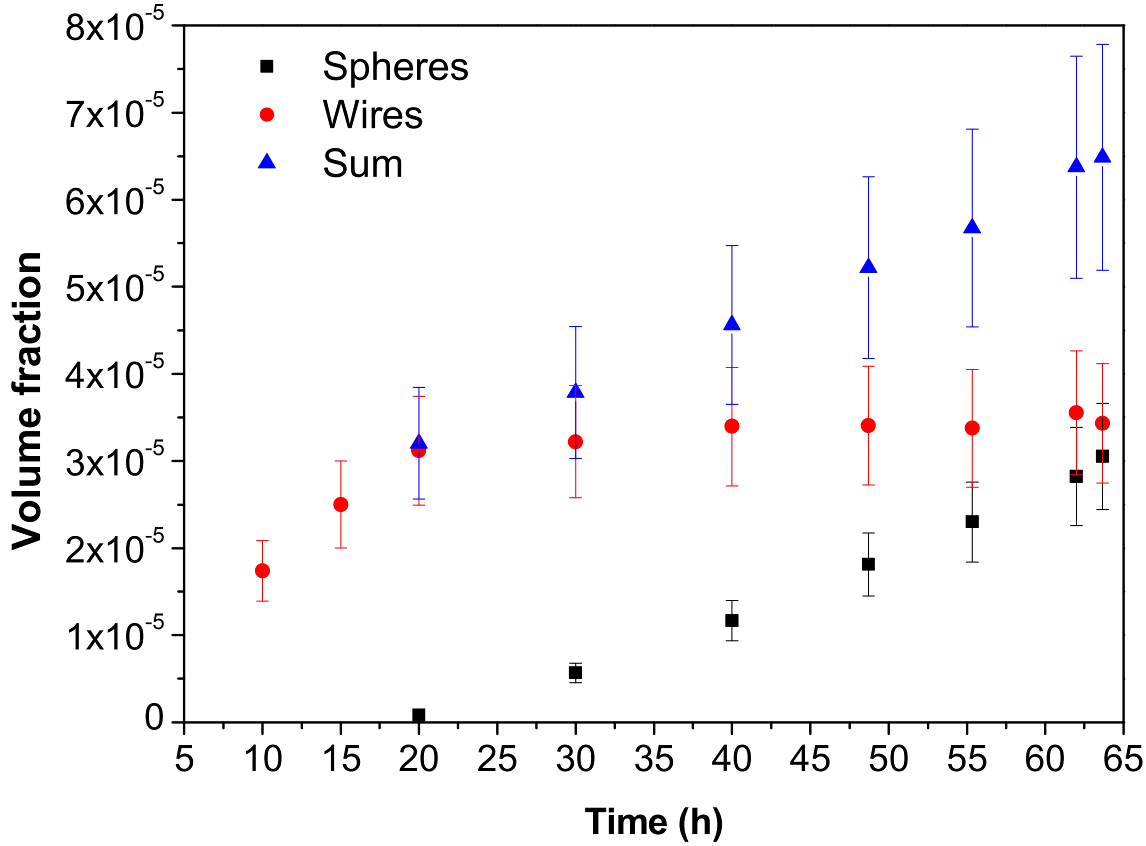

Spheres
Wires
Sum
Volume fraction
0
1x10^-5
2x10^-5
3x10^-5
4x10^-5
5x10^-5
6x10^-5
7x10^-5
8x10^-5
5 10 15 20 25 30 35 40 45 50 55 60 65
Time (h)

Figure 6

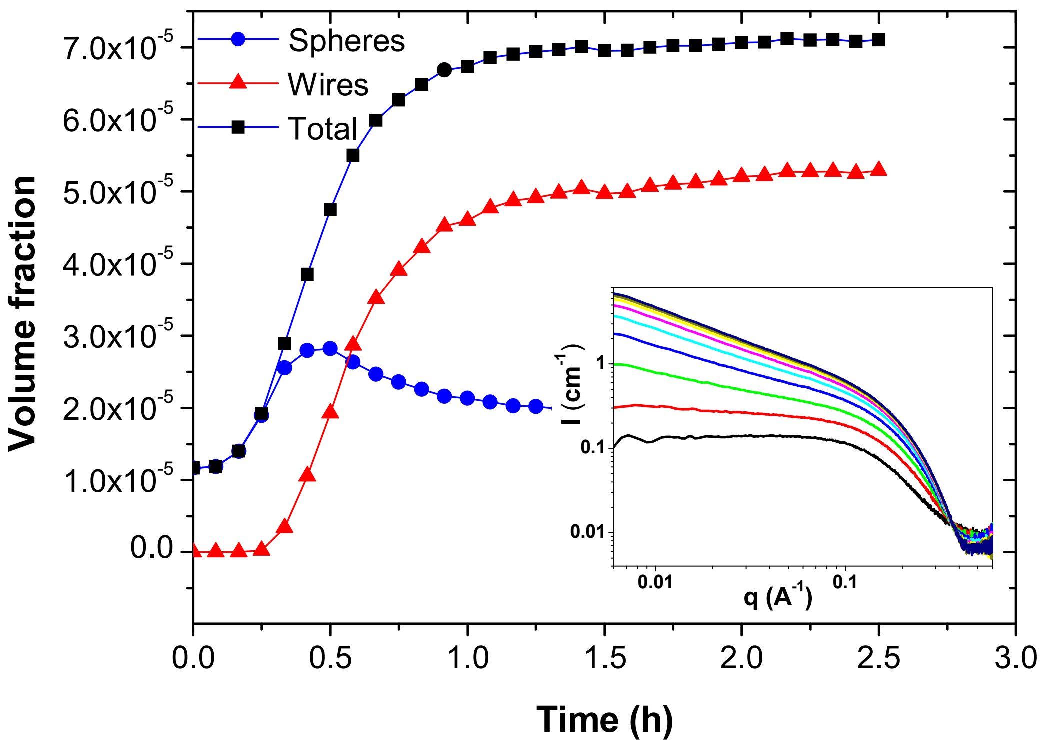
Spheres
Wires
Total
Volume fraction
7.0x10^-5
6.0x10^-5
5.0x10^-5
4.0x10^-5
3.0x10^-5
2.0x10^-5
1.0x10^-5
0.0
0.0
0.5
1.0
1.5
2.0
2.5
3.0
Time (h)
I (cm^-1)
1
0.1
0.01
0.01
0.1
q (A^-1)

Figure 7

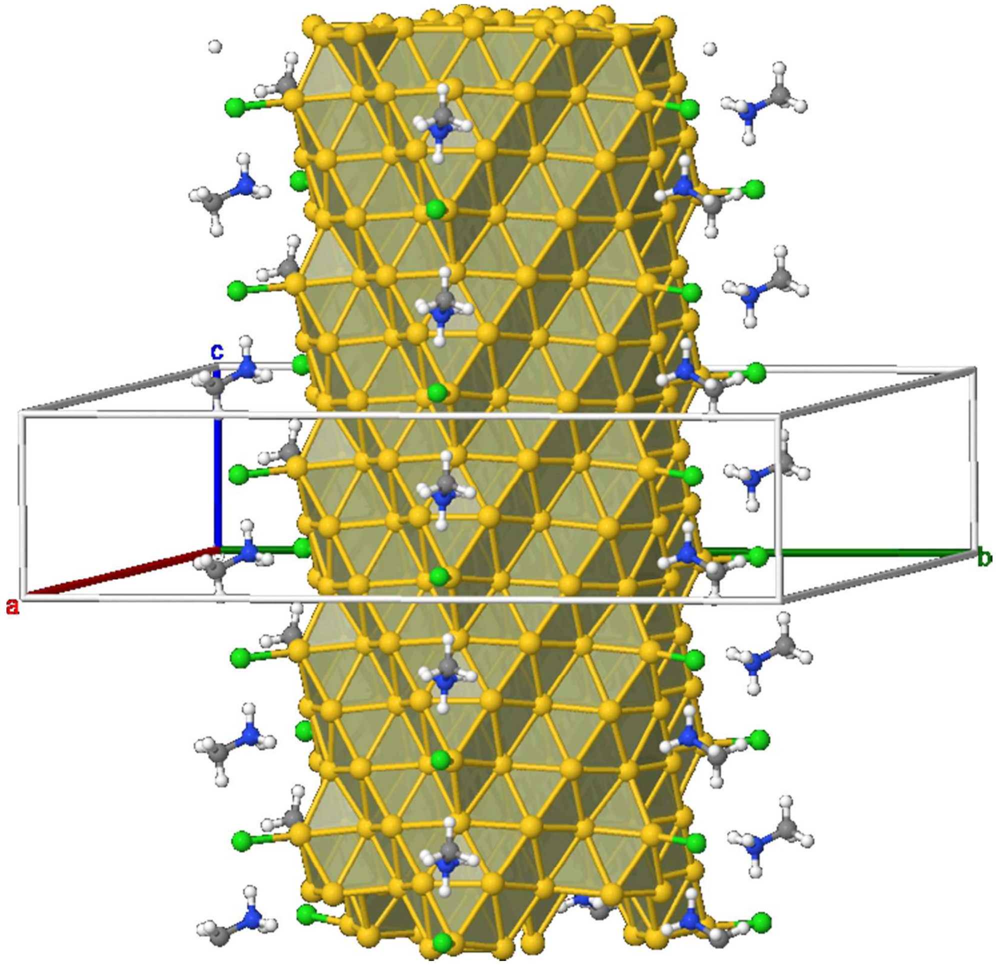

Figure 8

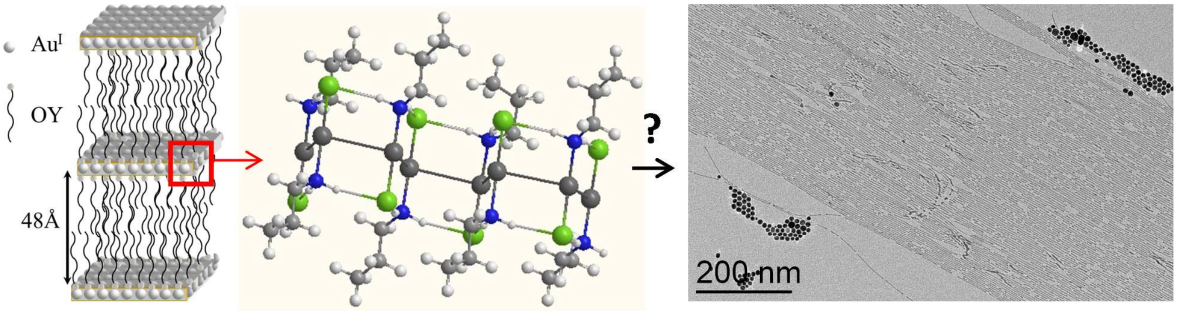

TOC